PCCP

Phase transition kinetics of LiNi0.5Mn1.5O4 analyzed by temperature-controlled operando X-ray absorption spectroscopy

Journal:	*Physical Chemistry Chemical Physics*
Manuscript ID	CP-ART-09-2015-005535.R2
Article Type:	Paper
Date Submitted by the Author:	02-Dec-2015

Complete List of Authors:	Takahashi, Ikuma; Kyoto University, Office of Society-Academia Collaboration for Innovation Arai, Hajime; Kyoto University, Office of Society-Academia Collaboration for Innovation Murayama, Haruno; Kyoto University, Office of Society-Academia Collaboration for Innovation Sato, Kenji; Kyoto University, Office of Society-Academia Collaboration for Innovation Komatsu, Hideyuki; Kyoto University, Office of Society-Academia Collaboration for Innovation Tanida, Hajime; Kyoto University, Office of Society-Academia Collaboration for Innovation Koyama, Yukinori; Kyoto University, Office of Society-Academia Collaboration for Innovation Uchimoto, Yoshiharu; Kyoto University, Graduate School of Human and Environmental Studies Ogumi, Z; Kyoto University, Office of Society-Academia Collaboration for Innovation

Journal Name

ARTICLE

Phase transition kinetics of $LiNi_{0.5}Mn_{1.5}O_4$ analyzed by temperature-controlled *operando* X-ray absorption spectroscopy

Received 00th January 20xx,
Accepted 00th January 20xx

DOI: 10.1039/x0xx00000x

www.rsc.org/

Ikuma Takahashi,†[a] Hajime Arai,[a] Haruno Murayama,‡[a] Kenji Sato,§[a] Hideyuki Komatsu,[a] Hajime Tanida,[a] Yukinori Koyama,[a] Yoshiharu Uchimoto[b] and Zempachi Ogumi[a]

LiNi0.5Mn1.5O4 (LNMO) is a promising positive electrode material for lithium ion batteries since it shows high potential of 4.7 V vs. Li/Li+. Its charge-discharge reaction includes two consecutive phase transitions between LiNi0.5Mn1.5O4 (Li1) ↔ Li0.5Ni0.5Mn1.5O4 (Li0.5) and Li0.5 ↔ Ni0.5Mn1.5O4 (Li0) and the complex transition kinetics that governs the rate capability of LNMO can hardly be analyzed by simple electrochemical techniques. Here we apply temperature-controlled operando X-ray absorption spectroscopy to directly capture the reacting phases at -20 °C to 40 °C under potential step (chronoamperometric) conditions and evaluate the phase transition kinetics using apparent first-order rate constants at various temperatures. The constant for the Li1 ↔ Li0.5 transition (process 1) is larger than that for the Li0.5 ↔ Li0 transition (process 2) at all the measured temperatures, and the corresponding activation energy values are 29 and 46 kJ mol-1 for processes 1 and 2, respectively. The obtaiend results are discussed to elucidate the limiting factor in this system as well as in other electrode systems.

Introduction

$LiNi_{0.5}Mn_{1.5}O_4$ (LNMO) is attractive as an electrode active material for lithium ion batteries that provides high energy density with high operating potential. [1, 2] In addition to its crystal structure and durability during charge-discharge cycling, [3-6] its rate capability, one of the important performances in the actual battery, has been analyzed and discussed. Practically, the effects of the particle size, [7, 8] lithium diffusivity [9-11] and substitution/coating modification [12, 13] on the rate capability of LNMO have been so far examined. For further improvement, it is indispensable to understand the rate determining step (or limiting factor) for the high rate operation.

In our previous reports, we have studied the phase transition behaviour of LNMO and have revealed that the phase transition is chiefly the rate determining step in the charge-discharge process. [14, 15] In contrast to the $LiFePO_4$ (LFP) electrode that essentially accompanies with single two-phase coexistence, [16, 17] the phase transition behavior of the LNMO electrodes is much complicated because there are two consecutive phase transitions at nearly the same potential (around 4.7 V vs. Li/Li^+), namely $LiNi_{0.5}Mn_{1.5}O_4$ (Li1 with Ni^{2+}) ↔ $Li_{0.5}Ni_{0.5}Mn_{1.5}O_4$ (Li0.5 with Ni^{3+}) and of Li0.5 ↔ $Ni_{0.5}Mn_{1.5}O_4$ (Li0 with Ni^{4+}) in low and high potential plateaus, respectively. [18-20] Accordingly it is difficult to analyze the behavior by simple electrochemical techniques [12] and it is desirable to directly capture the appearance and disappearance of each phase for detailed kinetics study. To elucidate the phase transition kinetics in a quantitative manner, we have employed X-ray absorption spectroscopy (XAS), which can directly trace the changes of the nickel oxidation state, under potential step (chronoamperometry) conditions at room temperature. [14] It has been shown using the changes of the Li1, Li0.5 and Li0 phase fractions with time that both of the Li0 ↔ Li0.5 and Li0.5 ↔ Li0 transitions apparently follow the first-order reaction kinetics and the rate constants can be obtained by analyzing the spectrum changes. However, the kinetic parameters obtained in our previous study [14] can hardly be compared and discussed with other data due to the lack of temperature control in the experimental system. By controlling the reaction temperature, the rate constants at various temperatures as well as the activation energy of the rate determining step can be evaluated. The

[a] *Office of Society-Academia Collaboration for Innovation, Kyoto University, Gokasho, Uji-shi, Kyoto 611-0011, Japan*
[b] *Graduate School of Human and Environmental Studies, Kyoto University, Yoshida-nihonmatsu-cho, Sakyo-ku, Kyoto 606-8501, Japan*
Present Addresses
†: *Nissan Research Center, Nissan Motor Co., Ltd, 1, Natsushima-cho, Yokosuka-shi, Kanagawa 237-8523, Japan*
‡: *Department of Chemistry, Faculty of Sciences, Kyusyu University, Hakozaki 6-10-1, Higashi-ku, Fukuoka 812-8581, Japan*
§: *Automobile R&D Center, Honda R&D Co., Ltd, 4630, Shimotakanezawa, Haga-machi, Haga-gun, Tochigi 321-3393, Japan*
Electronic Supplementary Information (ESI) available: [Equations used for obtaining rate constants, *operando* XAS measurement system, Current-time curves in potential step charging and discharging experiments, and examples of XANES spectra obtained after potential step charging at 40 °C].
See DOI: 10.1039/x0xx00000x

activation energy is generally free from physical parameters of the active material such as the particle size and surface morphology [21] (that can affect the apparent reaction rates) and thus is essential to discuss the reaction kinetics. The comparison of the activation energy with that of other possible limiting factors will lead to better understand of the reactions occurring in the battery. In addition, the overpotential from the equilibrium state that can affect the reaction kinetics [22] needs to be carefully controlled for the assessment of the kinetic parameter and reaction routes for charging and discharging.

In this study, we report the phase transition kinetics of LNMO analyzed by using newly established temperature-controlled *operando* XAS equipment that can directly capture the species of interest during the phase transition. The X-ray absorption near-edge structure (XANES) spectra were measured during charging and discharging at various temperatures and the rate constants were systematically evaluated with appropriate overpotential control. The activation energy associated with the phase transition is estimated in the temperature ranges of between -20 and 40 °C, where commercial batteries are practically operated. The obtained results are discussed in relation to the primary origin of the rate determining step in the phase transitions and comparison with other possible limiting factors occurring in the battery (i.e. the significance of phase transitions in the battery reactions), together with some perspectives.

Experimental

Sample preparation

The working composite electrode consisted of powder of $LiNi_{0.5}Mn_{1.5}O_4$ (Toda Kogyo) classified under 15 µm, acetylene black as a conductive additive and polyvinylidene difluoride as a binder, mixed in a 80:15:5 wt% ratio and coated on an aluminum current collector. This LNMO powder was mostly categorized as the disordered phase (>90%), proven by neutron diffraction.[14] The thickness of the working electrode was about 25 µm to minimize the liquid phase ion migration resistance in the electrode immersed in the electrolyte. [15, 23] The aluminium pouch-type cell used for *operando* measurements consisted of a working electrode (30 mm by 15 mm), metallic lithium foil as counter and reference electrodes, and a 1 mol dm^{-3} $LiPF_6$ solution of ethylene carbonate and ethylmethyl carbonate (3:7) as the electrolyte. A polyolefin film was used as a separator.

Electrochemical measurement

The potential step experiments to elucidate the phase transition kinetics of the electrode material were employed with temperature-controlled electrochemical equipment set at -20, -10, 0, 10, 25, and 40 °C. The potential for charging and discharging was carefully controlled as described previously. [15] Assuming that 4.72 V is the potential where the Li0.5 phase is thermodynamically stable, we set 4.85 V and 4.59 V as the potential values for charging and discharging where the Li0 and Li1 phases are respectively thermodynamically stable. The potentiostatic charging or discharging condition was kept for 1800 s. As shown below, this was enough for the full transition to Li0 and Li1 for charging and discharging, respectively, at room temperature and above. The initial states of the cells were set at room temperature before the potential step experiments at various temperatures, namely, the fully discharged state obtained by 0.1 C discharging to 3.50 V for the charging experiments and the fully charged state by 0.1 C charging to 4.85 V for the discharging experiments. To avoid the temperature history of the cell, a cell was used exclusively for a single measurement and not reused in other measurements. The capacity of the cells was approximately 120 mAh g^{-1} (82% utilization of theoretical capacity) at 0.1 C rate in the potential range from 3.50 to 4.85 V measured at room temperature. The capacity error among the cells was within ±1%.

Operando XAS analysis

Operando XAS was performed in a transmission mode with an electrochemical cell set in a temperature controlled jacket (see Figure S1) at BL-28XU of SPring-8, Hyogo, Japan. The XANES spectrum was measured in 8 s with the interval of another 8 s and the beam size was 1.5 mm by 2.0 mm, using ionization chambers as the detector. According to the previous study, the Ni *K*-edge energy values of 8349, 8351 and 8353 eV were used to trace the Ni^{2+}, Ni^{3+} and Ni^{4+} components, namely the Li1, Li0.5 and Li0 phases. [14] We determine each phase fraction during the potential step experiment by fitting these three components using the REX program package (Rigaku Co.).

Results

Figures 1 (a) and 1 (b) show capacity-time curves in the potential step charging and discharging experiment, respectively (see the corresponding current-time curves in Figure S2). The initial slope in these plots corresponds to the reaction rate at each temperature; 18 C (with 70% capacity), 6 C (with 40% capacity) and 1.3 C (with 20% capacity) are obtained for charging at 40 °C, 10 °C and -10 °C whereas 9 C (with 70% capacity), 3 C (with 40% capacity) and 0.8 C (with 20% capacity) are obtained for discharging at 40 °C, 10 °C and -10 °C. This indicates that the possible rate greatly depends on the temperature and higher rates are obtained for charging than discharging. The LNMO electrode is known to be a reversible system, however, these results show clear asymmetry in rate capability between charging and discharging, suggesting the effect of phase transition kinetics on the charge-discharge performance. We thus analyze the *operando* XANES spectra to detail the behavior of each phase.

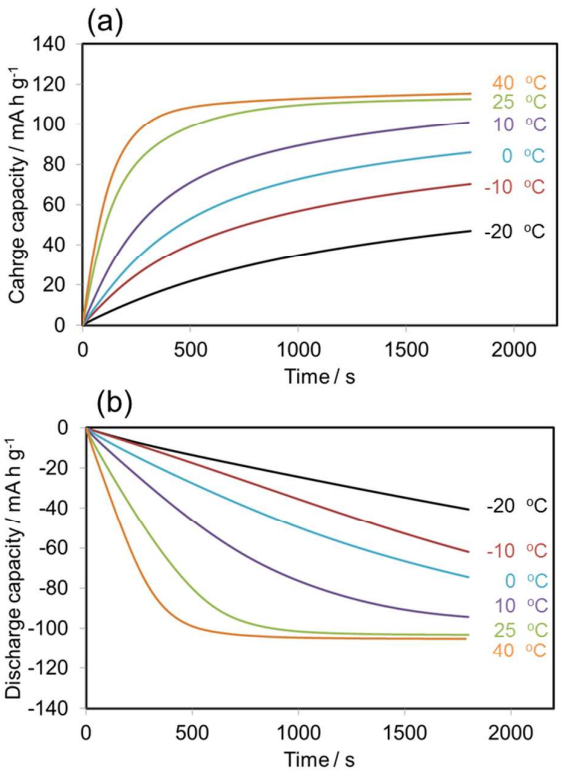

Figure 1 Capacity-time curves in potential step (a) charging and (b) discharging experiments.

The fractional changes of each phase with time were obtained by XANES spectrum deconvolution. [14] As an example, Figure S3 shows the XANES spectra for charging at 40 °C that consist of the fractions of (Li1, Li0.5, Li0) of (78%, 22%, 0%), (19%, 61%, 20%), and (0%, 22%, 78%) at 40, 120, and 400 s after the potential step, respectively. Other phase fractions during the potential step charging were similarly evaluated by the XANES spectra fitting.

The results at 40, 10 and -10 °C are shown as dots in Figures 2 (a), (b) and (c) respectively. The phase transition manner is similar to each other at all the temperatures, namely, the charging reaction sequentially proceeds from Li1 to Li0 via Li0.5 and there is a maximum in the fraction of Li0.5 where Li1 gradually disappears and Li0 starts to appear. However, the transition speeds are strongly temperature dependent; the fraction of Li0.5 reaches the maximum at 100 s after the potential step at 40 °C whereas it occurs much slowly at 1000 s after the potential step at -10 °C, indicating the significant effect of phase transition kinetics. The phase transition is complete in 600 s at 40 °C, which corresponds to the end of charging shown in Figure 1 (a), while Li0.5 remains and the phase transition is incomplete in 1800 s at low temperatures. Figure 3 shows the comparison between the measured charge capacity (solid curves, from Figure 1) and the integrated capacity deduced from the phase fractions obtained by XANES fitting (dots, from Figure 2) assuming that the capacities of 0.5

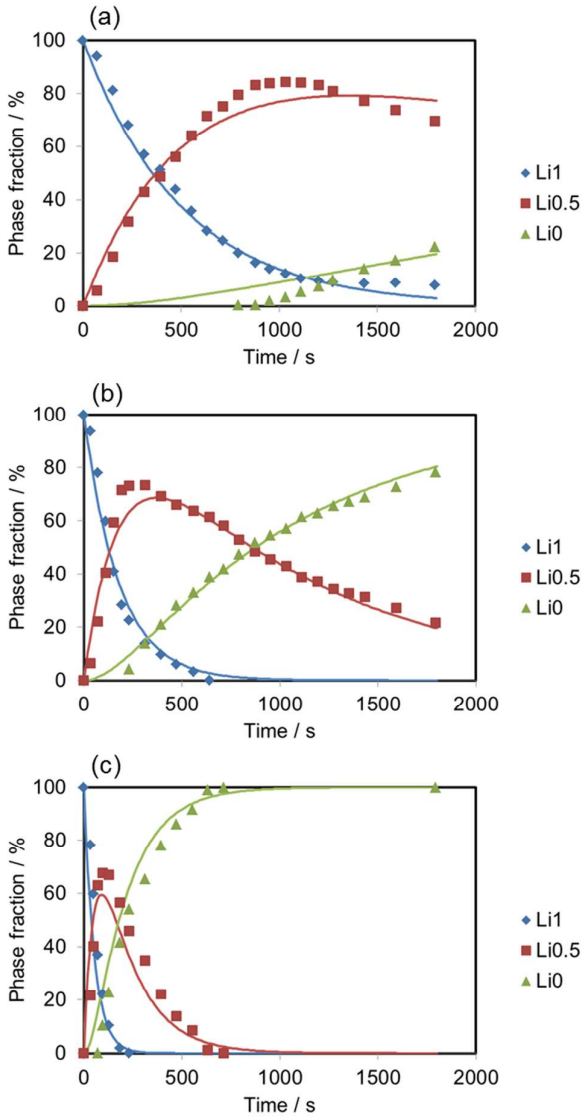

Figure 2 Phase fractions of $LiNi_{0.5}Mn_{1.5}O_4$ (Li1, diamond), $Li_{0.5}Ni_{0.5}Mn_{1.5}O_4$ (Li0.5, square) and $Ni_{0.5}Mn_{1.5}O_4$ (Li0, triangle) during potential step charging experiments at (a) 40 °C, (b) 10 °C and (c) -10 °C. The dots and the solid curves are the fractions evaluated using the XANES spectra and those calculated assuming first-order transition kinetics, respectively.

e and 1.0 e are required for the Li0.5 and Li0 formation, respectively. The capacity changes with time are roughly in agreement, showing that parasitic reactions, such as possible electrolyte oxidation during charging at 4.85 V, are insignificant even at 40 °C and the XANES spectra capture all the species involved in the electrochemical reactions.

It has been shown that the phase transitions kinetics in this system at room temperature can be expressed by two consecutive first-order reactions and the fractional changes of each phase with time can be obtained by solving the kinetic

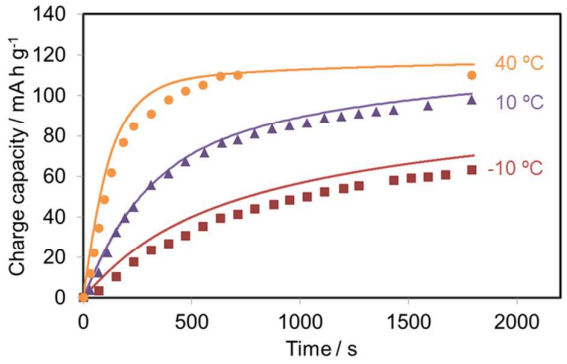

Figure 3 Capacity-time curves in potential step charging experiment experiments at 40 (circle), 10 (triangle) and -10 °C (square). The dots and the solid curves are the capacities evaluated using the XANES spectra and those based on the passed current, respectively.

equations using the rate constants k_1 and k_2 (see equations in Electronic Supplementary Information). [14]

$$[\mathrm{Li1}] \xrightarrow{k_1} [\mathrm{Li0.5}] \xrightarrow{k_2} [\mathrm{Li0}]$$

Now we extend these equations to other temperatures and the reaction rate constants k_1 and k_2 are determined by least square fitting to the phase fraction changes of Li1, Li0.5 and Li0 at each temperature. The resultant k_1 and k_2 values are shown in Table 1. The phase fractions using these rate constants are shown with solid lines in Figure 2, indicating good fits between the plots from the XANES measurements and lines from the calculation. This confirms that the phase transition behavior at each temperature is quantitatively expressed by the different first-order reaction rate constants. Note that k_1 is larger than k_2 at all the temperatures. It is now shown that the current responses shown in Figure 1 are governed by the phase transition kinetics because the same kinetic equations (with different rate constants) can well describe the transitions as shown in Figure 2, which in turn match the current responses match as shown in Figure 3. The ion transportation in the electrolyte is often the rate determining step in lithium ion batteries, [23] however, when thin composite electrodes are used that are effective in minimizing the reaction inhomogeneity, phase transitions in the solid phase can determine the rate, as shown above.

Table 1 Rate constant obtained from *operando* XANES data at each temperature.

Temperature / °C	$k_1 \times 10^3$ / s^{-1}	$k_2 \times 10^3$ / s^{-1}	$k_3 \times 10^3$ / s^{-1}	$k_4 \times 10^3$ / s^{-1}
-20	1.4	-	0.10	-
-10	2.0	0.17	0.20	-
0	3.8	0.47	0.42	-
10	5.6	1.0	0.91	-
25	11	3.1	2.7	7.1
40	19	5.7	6.3	10

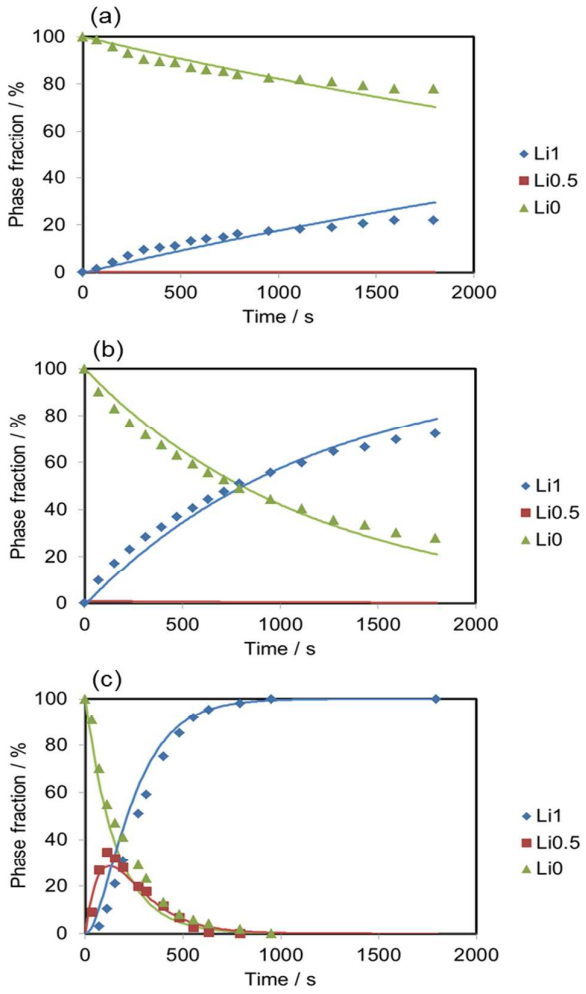

Figure 4 Phase fractions of Li1 (diamond), Li0.5 (square) and Li0 (triangle) during potential step discharging experiments at (a) 40 °C, (b) 10 °C and (c) -10 °C. The dots and the solid curves are the fractions evaluated using the XANES spectra and those calculated assuming first-order transition kinetics, respectively.

Dots in Figures 4 (a), 4 (b) and 4 (c) shows the phase fractions during the potential step discharging at 40, 10 and -10 °C, respectively, obtained by the XANES spectrum fitting. At 40 °C, the discharging reaction sequentially proceeds as Li0 → Li0.5 → Li1, being similar to the charge reaction, however, only Li1 and Li0 are observed and Li0.5 is absent at 10 and -10 °C. These phenomena qualitatively agree with the behavior of the XRD profiles observed in the LNMO system at low temperatures. [15]

Figure 5 shows the comparison between the measured discharge capacity (Figure 1 (b)) and the integrated capacity calculated from the phase fractions obtained by XANES fitting (Figure 4). The fit is good at 40 °C in all the time region. For lower temperatures, the fit is fine in the first 500 s (ca. 10 min), however, there is discrepancy in the latter part, in contrast to charging process. The origin of this discrepancy is unclear at the moment; imperfect XANES fitting due to

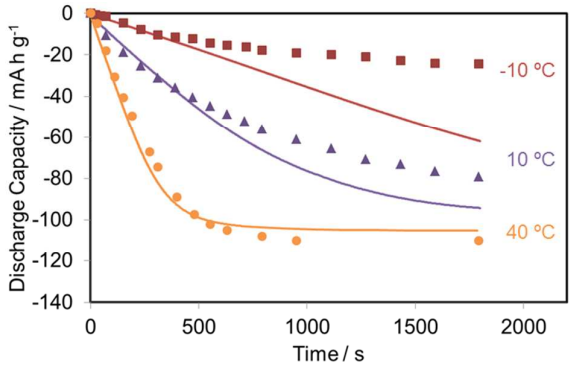

Figure 5 Capacity-time curves in potential step discharging experiment experiments at 40 (circle), 10 (triangle) and -10 °C (square). The dots and the solid curves are the capacities evaluated using the XANES spectra and those based on the passed current, respectively.

inevitable domain separation (Li0 and Li1) on discharging at low temperatures could cause an underestimated loss of Li0. Since the phase transition can well explain the current response at least in the first 500 s at all the temperatures, we now attempt to express the phase transitions kinetics during discharging also using two consecutive first-order reactions as follows.

$$[\mathrm{Li0}] \overset{k_3}{\rightarrow} [\mathrm{Li0.5}] \overset{k_4}{\rightarrow} [\mathrm{Li1}]$$

These equations for discharging can be solved as well as the equations for charging described above and the reaction rate constants k_3 and k_4 are determined by least square fitting to the phase fraction changes of Li1, Li0.5 and Li0 at each temperature (see equations in Electronic Supplementary Information). The invisible intermediate Li0.5 at low temperatures indicates that the rate determining step is Li0 →Li0.5 and the formed Li0.5 is instantly transformed into Li1. In these cases the rate constants k_3 can be obtained by the disappearance of Li0 whereas k_4, which should be much larger than k_3, cannot be adequately evaluated.

The best fitted values of k_3 and k_4 (if any) are shown in Table 1. At temperatures where k_4 is available, the relationship of k_3 < k_4 is apparent. When comparing these rate constants obtained during discharging with those obtained during charging, the k_1 and k_4 values are in the same order and this is also true for the k_2 and k_3 values, suggesting that the reaction pathway for each phase transition is essentially the same for charging and discharging. This implies that the phase transition proceeds essentially via the intermediate Li0.5 phase, though the transition is apparently direct from Li0 to Li1 for discharging at low temperatures. It is deduced from the finite k_1 values that some Li0.5 are not instantly transformed to Li1 on discharging even at low temperatures and the presence of obscure Li0.5 could explain the underestimated XANES-derived capacity in the latter part of discharging shown in Figure 5. A close inspection of the element spectrum (particularly of the

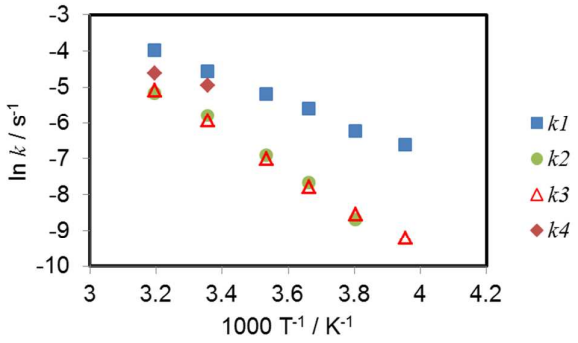

Figure 6 Arrhenius plots of rate constants. k_1, k_2, k_3 and k_4 values are shown as squares, circles, triangles and diamonds, respectively.

Li0.5 phase) could improve the fitting. Note that k > 0.06 s^{-1} cannot be properly determined due to the time resolution of the XANES measurement (16 s) and the k values obtained here are all below this limit even at high temperatures.

Figure 6 summarizes the temperature dependence of the k values in an Arrhenius plot. The activation energy E_{a1} for the Li1↔Li0.5 transition and E_{a2} for the Li0.5↔Li0 transition are evaluated from the slope of Arrhenius plots using these k values and they are respectively 26 and 49 kJ mol^{-1}, showing large difference between the two activation barriers.

A reaction scheme derived from the activation barriers is shown in Fig. 7. This indicates that at high temperatures the phase transitions are facile and proceed stepwise for both charging and discharging. On the other hand at low temperatures, the charging process stops at Li0.5 due to the higher activation barrier for the Li0.5↔Li0 transition (E_{a2}) whereas the majority of Li0 remains unreacted with some active species jumping to Li1 during the discharging process because the active species that surpasses the high activation barrier (E_{a2}) can immediately get over the low activation barrier (E_{a1}), leading to the absence of Li0.5.

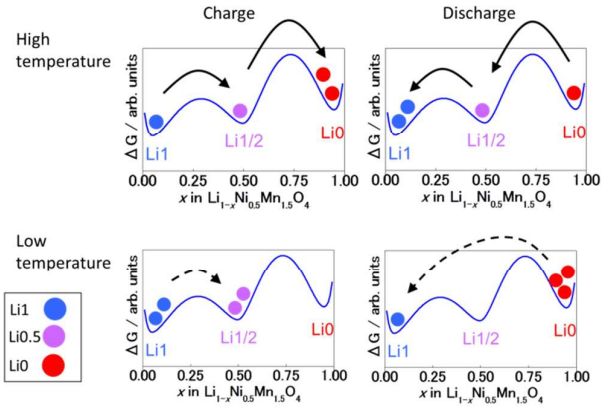

Figure 7 Charge-discharge reaction scheme of LNMO at high and low temperatures. The blue hills correspond to the activation barriers in the phase transitions.

The coexistence of the Li0 and Li1 phases in the discharged state at low temperatures implies that there is reaction distribution and a part of the electrode (the Li1 portion) is utilized during the repeated charge-discharge cycles while the rest (the Li0 portion) is kept in the high oxidation state (Ni^{4+}). Such inhomogeneous utilization of the electrode material can lead to fast degradation, when compared to the homogeneously utilized conditions.

Discussion

(1) Primary rate determining step in phase transitions

The obtained current is determined by the phase transition kinetics, more precisely the first-order rate constants *k* as described above. With the analogy of the LFP electrode that has been analyzed by the Avrami equations, [16, 21, 22] it is deduced that the primary rate determining step is either the rearrangement of the chemical bonds at the reaction interface or the two-dimensional lithium diffusion in the phase boundary plane. Of the two possibilities, the latter seems more probable because slow movement of the phase transition front (boundary) has been recently shown by *operando* XRD study of LNMO. [24] This means that the *k* values represent the speed of the phase boundary movement. As shown later, LNMO with three-dimensional lithium paths in the spinel structure and LFP with one-dimensional lithium diffusion paths in the olivine structure have comparable activation barriers for the phase transition, suggesting that the rearrangement of the chemical bonds at the reaction interface (i.e. the phase boundary movement) is the primary factor.

(2) Different activation barriers for two transitions

The large difference between the two activation energy values is surprizing because the Li1, Li0.5 and Li0 phases all have the same spinel structures. Considering the lattice parameters of Li1 (8.17 Å), Li0.5 (8.08 Å) and Li0 (8.00 Å), the volume changes between the phases are both ca. 3%.

Though the true reason for the large difference in $E_{a1} < E_{a2}$ is unclear at the moment, there are a few possibilities, namely, structural, electronic and transportation factors. The structural factor is based on that there is a thermodynamically stable solid solution region in the Li1↔Li0.5 transition [25, 26] that can mitigate the lattice deformation while there is no such region in the Li0.5↔Li0 transition, though *operando* XRD study shows diffusing lattice constants in non-equilibrium states. [24] The second one is due to the redox of Ni^{3+}↔Ni^{4+} being slower than Ni^{2+}↔Ni^{3+}. Since Ni^{4+} (d^6, low spin) oxidized from Ni^{3+} (d^7, low spin) [18] has no electron in the conduction band, the limited electron transfer in the lattice could result in the slow transition. The transportation limitation is related to slow lithium diffusion in the lattice [23] as will be described later. Further study is needed to clarify the true reason for $E_{a1} < E_{a2}$.

It is interesting to note that the stepwise kinetic equations well explains the XANES spectrum changes even at high rates (e.g. in the beginning of experiments at 40 °C) while the XRD analysis indicates the diffusing lattice changes in non-equilibrium states, particularly at high rates. [24] This suggests that distinct valence states of Ni^{2+}, Ni^{3+} and Ni^{4+} are involved throughout the charging/discharging processes, even in the intermediate states of LNMO. The similar behavior has been reported also for LFP that a stepwise phase transition is observed by XAS analysis while various intermediates are shown by XRD. [17, 27] It is also noted that $Na_{2/3}FePO_4$, an intermediate between $NaFePO_4$ and $FePO_4$, is reported to contain ordered Fe^{2+} and Fe^{3+} species in the structure. [28]

(3) Comparison with other limiting factor in batteries

Here we compare the obtained activation energy for the phase transitions with the reported activation barriers of other possible rate determining factors in the battery reactions that govern the rate capability, to better understand the limiting factors in battery operation.

The barriers for lithium diffusion in the LNMO latticed based on density functional theory calculation have been reported to be 30 to 52 kJ mol^{-1} depending on the diffusion paths in the lattice. [23] Unfortunately the values cannot be directly compared with the present results because the existence of Li0.5 is not considered in this calculation. Though the phase transition seems to be the essential limiting factor as described above, the effect of the lithium diffusion in the electrode material could also affect the electrode kinetics when considering the comparable activation barrier for the lithium diffusion.

The activation barrier for the electron conduction, caused by thermally-assisted polaron hopping between nickel ions, has recently been reported to be 30-40 kJ mol^{-1}.[29] As has inferred there, this step is basically not rate determining in the composite electrode containing a sufficient amount of conductive agents (15% in weight in our electrode).

A well-known limiting factor in the battery reactions is the charge transfer at the interface between the electrode and electrolyte. For various lithium transport systems in contact with organic electrolytes, the solvation-desolvation reactions are considered as the slowest step and the activation energy values are generally around 50 kJ mol^{-1} [32-34], though there are a few exceptional cases with smaller activation energy values [35, 36]. Despite the high activation barrier for the charge transfer, it is expected that the phase transitions are the primary limiting factor in the present case because the asymmetric behavior shown in Fig. 7 can hardly be explained by the charge transfer limitation. Large frequency factors for the charge transfer could result in the apparent insensitivity of the charge transfer to the present case, which implies that the charge transfer could be rate determining at extremely low temperatures.

The reported activation energy for lithium diffusion in the organic electrolytes of 11-16 kJ mol^{-1} [37] is much smaller than the phase transition barriers and so the lithium diffusion in the electrolytes is not the limiting factor when thin electrodes such as those used in this study are applied. Note that in thick electrodes the lithium diffusion in the tortuous paths can be rate determining [23] and can cause reaction inhomogeneity inside the electrode and capacity loss. [38]

The comparison among the activation barriers can contribute to the better design and control of batteries used in wide temperature ranges such as those for electric vehicles. From another point of view, the activation energy for these barriers

are mostly below 50 kJ mol^{-1}, suggesting that more sluggish kinetics are not allowable for practical battery application.

(4) Comparison of activation barriers with other electrodes

Here we compare the obtained activation energy of the LNMO with that of other two-phase coexistence electrode systems. The activation energy for the transition $LiFePO_4 \leftrightarrow FePO_4$ is reported to be 33, [30] 34-41, [29] and 40-42 [22] kJ mol^{-1}. Besides, the activation energy of 41 kJ mol^{-1} has been reported for $Li_{1+x}Mn_2O_4$, which is generally considered to be a slow two-phase reaction system. [31] Comparing with these values, the energy for the transition of Li1 ↔ Li0.5 in LNMO is smaller and that of Li0.5 ↔ Li0 is larger. This suggests that the former transition is facile and can produce sufficient capacity even at low temperatures while the latter is slow and can cause considerable capacity reduction at low temperatures.

(5) Application to other materials and fields

The developed method can essentially be applied to obtain the activation energy and the related kinetic information of electrochemical reactions that involve transition metal valence changes with time. For example, it would be interesting to apply the present analysis to the kinetics of partially substituted LNMO that are reported to have higher rate capability than the pristine LNMO [12, 13], which can provide more insight into the role of substitution. Possible application fields include not only battery materials but electrochromic reactions [39], catalytic reactions [40] and photovoltaic reactions. [41] For analyzing local reactions such as those at the catalyst surface, it is essential to ensure sufficient measuring area so that any reaction inhomogeneity, which can cause the spectrum interpretation difficult, is avoided.

Conclusions

The temperature-controlled *operando* XAS analysis is established to independently evaluate the two rate constants for the phase transitions in LNMO at various temperatures. The activation energies for Li1 ↔ Li0.5 (E_{a1}) and Li0.5 ↔ Li0 (E_{a2}) are 29 and 46 kJ mol^{-1}, respectively. This large difference in the activation energy affects the phase transition behavior; the symmetric transitions for charge and discharge at room temperature and above is no more seen at lower temperatures, causing the remaining Li0.5 on charging and unreacted Li0 on discharging. The rate determining step can be ascribed to the rearrangement of the chemical bonds at the reaction interface. The results indicates that the activation barrier for the phase transition is the primary limiting factor, however, other factors such as lithium diffusion in the lattice and the charge transfer reaction could also affect the rate capability.

The temperature-controlled *operando* XAS technique is suitable to directly track the behavior of the reacting species and to properly evaluate the activation energy of multi-phase reaction systems. It is expected that the information obtained in the kinetic study is useful in understanding the limiting factors and in obtaining the design guidelines for batteries and other applications.

Acknowledgements

This work was supported by Research and Development Initiative for Scientific Innovation of New Generation Batteries (RISING) project of NEDO (Japan). The synchrotron radiation experiments were performed with the approval of the Japan Synchrotron Radiation Research Institute (JASRI) (Proposal No.2010B1896, 2011A1013, 2011A1014, 2011B1034, 2012A7601, 2012B7601, 2013A7601). We thank Mr. T. Kakei for preparing samples and Ms. A. Wakita for data analysis.

Notes and references

1 K. Amine, H. Tsukamoto, H. Yasuda and Y. Fuiita, *J. Electrochem. Soc.*, 1996, **143**, 1607.
2 Q. Zhong, A. Bonakclarpour, M. Zhang, Y. Gao and J. R. Dahn, *J. Electrochem. Soc.*, 1997, **144**, 205.
3 M. Okada, Y.-S. Lee and M. Yoshio, *J. Power Sources*, 2000, **90**, 196.
4 D. Aurbach, B. Markovsky, Y. Talyossef, G. Salitra, H.-J. Kim and S. Choi, *J. Power Sources*, 2006, **162**, 780-789.
5 K. Ariyoshi, Y. Maeda, T. Kawai and T. Ohzuku, *J. Electrochem. Soc.*, 2011, **158**, A281.
6 S. Mukerjee, X. Q. Yang, X. Sunb, S. J. Lee, J. McBreen and Y. Ein-Eli, *Electrochim Acta*, 2004, **49**, 3373.
7 M. Kunduraciz and G. G. Amatucci, *Electrochim Acta*, 2008, **53**, 4193.
8 Y. Talyosef, B. Markovsky, R. Lavi, G. Salitra, D. Aurbach, D. Kovacheva, M. Gorova, E. Zhecheva and R. Stoyanova, *J. Electrochem. Soc.*, 2007, **154**, A682.
9 M. Mohamedi, M. Makino, K. Dokko, T. Itoh and I. Uchida, *Electrochim Acta*, 2002, **48**, 79.
10 J. Liu and A. Manthiram, *J. Electrochem. Soc.*, 2009, **156**, A833.
11 H. Xia, Y. S. Meng, L. Lu and G. Ceder, *J. Electrochem. Soc.*, 2007, **154**, A737.
12 J. Liu and A. Manthiram, *J. Phys. Chem. C*, 2009, **113**, 15073.
13 H. Wang, T. A. Tan, P. Yang, M. O. Lai and L. Lu, *J. Phys. Chem. C*, 2011, **115**, 6102.
14 H. Arai, K. Sato, Y. Orikasa, H. Murayama, I. Takahashi, Y. Koyama, Y. Uchimoto and Z. Ogumi, *J. Mater. Chem. A*, 2013, **1**, 10442.
15 I. Takahashi, H. Murayama, K. Sato, T. Naka, K. Kitada, K. Fukuda, Y. Koyama, H. Arai, E. Matsubara, Y. Uchimoto and Z. Ogumi, *J. Mater. Chem. A*, 2014, **2**, 15414.
16 J. L. Allen, T. R. Jow and J. Wolfenstine, *Chem. Mater.*, 2007, **19**, 2108.
17 Y. Orikasa, T. Maeda, Y. Koyama, H. Murayama, K. Fukuda, H. Tanida, H. Arai, E. Matsubara, Y. Uchimoto and Z. Ogumi, *Chem. Mater.*, 2013, **25**, 1032.
18 Y. Terada, K. Yasaka, F. Nishikawa, T. Konishi, M. Yoshio and I. Nakai, *J. Solid State Chem.*, 2001, **156**, 286.
19 J. Rana, S. Glatthaar, H. Gesswein, N. Sharma, J. R. Binder, R. Chernikov, G. Schumacher and J. Banhart, *J. Power Sources*, 2014, **255**, 439.
20 K. Dokko, M. Mohamedi, N. Anzue, T. Itoh and I. Uchida, *J. Mater. Chem.*, 2002, **12**, 3688.
21 Y. Orikasa, T. Maeda, Y. Koyama, T. Minato, H. Murayama, K. Fukuda, H. Tanida, H. Arai, E. Matsubara, Y. Uchimoto and Z. Ogumi, *J. Electrochem. Soc.*, 2013, **160**, A3061.
22 G. Oyama, Y. Yamada, R.-i. Natsui, S.-i. Nishimura and A. Yamada, *J. Phys. Chem. C*, 2012, **116**, 7386.
23 X. Ma, B. Kang and G. Ceder, *J. Electrochem. Soc.*, 2010, **157**, A925.
24 H. Komatsu, H. Arai, Y. Koyama, K. Sato, T. Kato, R. Yoshida, H. Murayama, I. Takahashi, Y. Orikasa, K. Fukuda, T.

Hirayama, Y. Ikuhara, Y. Ukyo, Y. Uchimoto and Z. Ogumi, *Adv. Energy. Mater.*, 2015, **5**, 1500638.
25 M. Kunduraciz and G. G. Amatucci, *J. Electrochem. Soc.*, 2006, **153**, A1345 - A1352.
26 K. Saravanan, A. Jarry, R. Kostecki and G. Chen, *Scientific report*, 2015, **5**, 8027.
27 Y. Orikasa, T. Maeda, Y. Koyama, H. Murayama, K. Fukuda, H. Tanida, H. Arai, E. Matsubara, Y. Uchimoto and Z. Ogumi, *J. Am. Chem. Soc.*, 2013, **135**, 5497.
28 F. Boucher, J. l. Gaubicher, M. Cuisinier, D. Guyomard and P. Moreau, *J. Am. Chem. Soc.*, 2014, **136**, 9144.
29 Z. Moorhead-Rosenberg, A. Huq, J. B. Goodenough and A. Manthiram, Chem. Mater., 2015, **27**, 6934.
30 T. Abe, H. Fukuda, Y. Iriyama and Z. Ogumi, *J. Electrochem. Soc.*, 2004, **151**, A1120.
31 T. Abe, F. Sagane, M. Ohtsuka, Y. Iriyama and Z. Ogumi, *J. Electrochem. Soc.*, 2005, **152**, A2151.
32 I. Yamada, K. Miyazaki, T. Fukutsuka, Y. Iriyama, T. Abe and Z. Ogumi, *J. Power Sources*, 2015, **294**, 460.
33 Y. Yamada, Y. Iriyama, T. Abe, Z. Ogumi, *J. Electrochem. Soc.*, 2010, **157**, A26.
34 M. Nakayama, H. Taki, T. Nakamura, S. Tokuda, R. Jalem and T. Kasuga, *J. Phys. Chem. C*, 2014, **118**, 27245.
35 P. Porion, Y. R. Dougassa, C. Tessier, L. El Ouatani, J. Jacquemin and M. Anouti, *Electrochim. Acta*, 2014, **114**, 95.
36 H. Murayama, K. Kitada, K. Fukuda, A. Mitsui, K. Ohara, H. Arai, Y. Uchimoto, Z. Ogumi and E. Matsubara, *J. Phys. Chem. C,* 2014, **118**, 20750.
37 T. R. Jow, M. B. Marx and J. L. Allen, *J. Electrochem. Soc.*, 2012, **159**, A604.
38 L. Liao, P. Zuo, Y. Ma, X. Q. Chen, Y. An, Y. Gao and G. Yin, *Electrochim Acta*, 2012, **60**, 269.
39 M. Okubo, Y. Mizuno, H. Yamada, J. Kim, E. Hosono, H. Zhou, T. Kudo and I. Honma, *ACS nano*, 2010, **4**, 741.
40 P. R. Bueno, C. Gabrielli and H. Perrot, *Electrochim. Acta*, 2008, **53**, 5533.
41 M. Tada, S. Murata, T. Asakoka, K. Hiroshima, K. Okumura, H. Tanida, T. Uruga, H. Nakanishi, S.-i. Matsumoto, Yasuhiro Inada, M. Nomura and Y. Iwasawa, *Angew. Chem. Int. Ed.*, 2007, **46**, 4310.
42 M. Yoshida, T. Yomogida, T. Mineo, K. Nitta, K. Kato, T. Masuda, H. Nitani, H. Abe, S. Takakusagi, T. Uruga, K. Asakura, K. Uosaki and H. Kondoh, *J. Phys. Chem. C*, 2014, **118**, 24302.